

Optimal Measurement Projections with Adaptive Mixture Kalman Filtering for GNSS Positioning

Greiff, Marcus; Berntorp, Karl

TR2020-097 July 03, 2020

Abstract

Accurate carrier-phase integer ambiguity resolution is fundamental for high precision global navigation satellite systems (GNSSs). In this paper we extend a recently proposed mixture Kalman filter solution to integer ambiguity resolution. We utilize the Fisher information matrix to project the acquired measurements into a lower-dimensional subspace, formulating an optimization program to find the projected measurement that minimally degrades filter performance with respect to the mean squared error (MSE) of the estimate. Using the projected measurements, our method achieves a significant computational speedup while retaining the performance of the original filter. Theoretical results are presented regarding the optimal projection computation, and the claims are subsequently illustrated by simulation examples in a Monte Carlo study

American Control Conference (ACC) 2020

Optimal Measurement Projections with Adaptive Mixture Kalman Filtering for GNSS Positioning

Marcus Greiff¹, Karl Berntorp¹

Abstract—Accurate carrier-phase integer ambiguity resolution is fundamental for high precision global navigation satellite systems (GNSSs). In this paper we extend a recently proposed mixture Kalman filter solution to integer ambiguity resolution. We utilize the Fisher information matrix to project the acquired measurements into a lower-dimensional subspace, formulating an optimization program to find the projected measurement that minimally degrades filter performance with respect to the mean squared error (MSE) of the estimate. Using the projected measurements, our method achieves a significant computational speedup while retaining the performance of the original filter. Theoretical results are presented regarding the optimal projection computation, and the claims are subsequently illustrated by simulation examples in a Monte Carlo study.

I. INTRODUCTION

Global navigation satellite systems (GNSS), such as GPS, Galileo, and, in the future, QZSS, are used in many positioning and navigation applications. A GNSS receiver determines its position using two types of range measurements from several satellites orbiting the Earth: pseudorange (or code) measurements and carrier-phase measurements. The code measurement is determined by multiplying the signal travel time from the satellite to the receiver with the speed of light, but becomes prone to several sources of errors. The carrier-phase measurement is obtained by integrating a reconstructed carrier of the signal as it arrives at the receiver. The carrier-signal observations are more precise than the code measurements and can be tracked within a percent or less of the carrier wavelength, $\lambda \approx 0.2$ [m], assuming all error sources have been corrected for. However, due to the unknown number of wave periods in transit between the satellite and the receiver, when the receiver starts tracking the carrier phase, there is an integer ambiguity in the carrier-phase measurement. Furthermore, a sudden loss of lock of the carrier signal, a so-called cycle slip, causes a jump in the carrier-phase measurements and is a common error source.

1) *Prior work*: An overview of traditional approaches for ambiguity resolution can be found in [1], and a summary of integer estimation theory is presented in [2]. Many GNSS ambiguity resolution methods are based on two-stage approaches. First an estimation of a real-valued ambiguity by an augmentation of the receiver state vector with the ambiguities, using the extended Kalman filter (EKF) [3] or least squares [2], forming the basis for an integer least squares (ILS) solution based on the real-valued estimates. An example of this is the LAMBDA method [4–6].

In contrast to these approaches, particle filters (PFs) have seen a lesser degree of success in GNSS positioning applications due to their computational complexity. In [7], [8] the integer estimates are formed using the position samples generated in the PF by manipulations of the likelihood. The work in [9] applies particle filtering for estimating the joint GNSS receiver state and ambiguities. However, estimating the joint state and ambiguities in a PF leads to a high-dimensional estimation problem, requiring a large amount of particles and computational resources. The approach in [10], [11], which this paper extends, differs from previous work in that the ambiguities are marginalized.

2) *Contribution*: In this paper, we propose to leverage the Fisher information matrix (FIM) [12] to reduce the computational complexity of the recursive measurement updates in [10], [11], while retaining the theoretical benefits of using a PF for the integer ambiguity resolution problem. In a typical GNSS application, the metric to be minimized is the mean squared error (MSE) of the positional estimate, and the fundamental performance bound of the filter is given by the corresponding Cramér Rao bound (CRB) [13]. Consequently, our approach expresses an objective function in terms of a change in the CRB of the positional MSE when using a set of linearly projected measurements, as a function of the projection operator used. If (i) the estimator yields performance approaching the CRB, and (ii) the projection is such that CRB of the positional MSE changes minimally when using the projected measurements, then we should expect almost identical performance in minimum MSE-filtering approaches with the full and the projected measurements. Our introduction of the projected measurements in this paper does not seek to improve the MSE performance of the filter in [11], but rather to reduce its computational complexity.

3) *Notation*: For a discrete time signal x with sampling period T_s , $x_k = x(t_k) = x(kT_s)$. For a vector-valued discrete time signal \mathbf{x} , $\mathbf{x}_{m:k} = \{\mathbf{x}_m, \dots, \mathbf{x}_k\}$ is the sequence of values of \mathbf{x} between sampling instants m and k , and $\hat{\mathbf{x}}_{h|k}$ denotes the estimated value of \mathbf{x} at time step h , based on data up to time step k . With $p(\mathbf{x}_{0:k}|\mathbf{y}_{0:k})$, we mean the posterior density function of the state trajectory $\mathbf{x}_{0:k}$ given the measurement sequence $\mathbf{y}_{0:k}$. As the filter in [11] concurrently runs a marginalized PF and an EKF bank, the index $(\cdot)^i$ will refer to a particle in the marginalized PF, and the index $(\cdot)^{\text{KF},i}$ to a particle in the EKF bank. We let \mathbb{R} and \mathbb{Z} denote the sets of real and integer numbers respectively. We let \mathbf{I} be the identity matrix, $\|\cdot\|_2$ denote l_2 -norm, and $\mathcal{N}(\mathbf{x}_k; \boldsymbol{\mu}_k, \boldsymbol{\Upsilon}_k)$ denote a Gaussian density function with mean $\boldsymbol{\mu}_k$ and covariance matrix $\boldsymbol{\Upsilon}_k$. With $\mathcal{U}(\mathbf{I})$ we mean

¹Control and Dynamical Systems, Mitsubishi Electric Research Laboratories, Ca, MA, 02139, USA. {greiff,berntorp}@merl.com

a uniform distribution over the interval I . Furthermore, $\mathbb{E}(\cdot)$ and $\text{Cov}(\cdot)$ denote an expectation and covariance of a random variable respectively. Finally, Ψ refers to a linear projection operator, and $\tilde{\mathbf{a}}$ denotes a projection of \mathbf{a} by Ψ .

II. PROBLEM SETUP

We consider the code and carrier-phase measurements from the j^{th} satellite to the receiver r at a time t_k , using the standard measurement model [2], [9], [14–16],

$$P_{r,k}^j = \rho_{r,k}^j + c(\delta t_{r,k} - \delta t_k^j) + I_{r,k}^j + T_{r,k}^j + \epsilon_{r,k}^j, \quad (1a)$$

$$\Phi_{r,k}^j = \rho_{r,k}^j + c(\delta t_{r,k} - \delta t_k^j) - I_{r,k}^j + T_{r,k}^j + \lambda n_{r,k}^j + \eta_{r,k}^j, \quad (1b)$$

where $P_{r,k}^j$ is the code measurement, $\rho_{r,k}^j$ is the distance between the receiver and the j^{th} satellite, c is the speed of light, $\delta t_{r,k}$ and δt_k^j are the receiver and satellite clock bias respectively. $I_{r,k}^j$ is the ionospheric delay, $T_{r,k}^j$ is the tropospheric delay, $\epsilon_{r,k}^j$ is the code observation noise, $\Phi_{r,k}^j$ is the carrier-phase observation, λ is the carrier wavelength, $n_{r,k}^j$ is the ambiguity, and $\eta_{r,k}^j$ is the carrier observation noise. The measurement noise is assumed Gaussian distributed $\epsilon_{r,k}^j \sim \mathcal{N}(0, \sigma_\epsilon^2)$, $\eta_{r,k}^j \sim \mathcal{N}(0, \sigma_\eta^2)$. The distance between the receiver and the j^{th} satellite is $\rho_{r,k}^j = \|\mathbf{p}_k^j - \mathbf{p}_{r,k}\|_2$, where $\mathbf{p}_k^j, \mathbf{p}_{r,k} \in \mathbb{R}^3$ are the coordinates of the j^{th} satellite and the receiver r respectively in ECEF coordinates [1].

By utilizing a base receiver (reference) b mounted at a known location broadcasting to the target receiver r , most of the error sources can be removed, or mitigated. Forming single or double differences (DD) of measurements from pairs of satellites and the receivers reduce the error source [16]. For very short distances between r and the base receiver b , the DD operation eliminates the ionospheric and tropospheric delays [9], [16]. For longer baselines (e.g., above 10 km) other methods can be used [17], [18] to reduce the delays.

Denote the single-differenced observation equations between the receivers b and r with $\Delta P_{br,k}^j = P_{b,k}^j - P_{r,k}^j$ and $\Delta \Phi_{br,k}^j = \Phi_{b,k}^j - \Phi_{r,k}^j$, respectively, and the DD between a reference (pivot) satellite l and satellite j with $\nabla \Delta (\cdot)_{br,k}^{jl}$. For short baselines or using delay estimators [17], [18],

$$\nabla \Delta P_{br,k}^{jl} \approx \nabla \Delta \rho_{br,k}^{jl} + \nabla \Delta \epsilon_{br,k}^{jl}, \quad (2a)$$

$$\nabla \Delta \Phi_{br,k}^{jl} \approx \nabla \Delta \rho_{br,k}^{jl} + \lambda \nabla \Delta n_{br}^{jl} + \nabla \Delta \eta_{br,k}^{jl}. \quad (2b)$$

We assume M pairs of observation equations of the form (2), where M can vary over different time steps, and introduce

$$\mathbf{n}_k = [\nabla \Delta n_{br,k}^{l1} \ \cdots \ \nabla \Delta n_{br,k}^{lM}]^\top \in \mathbb{Z}^M. \quad (3)$$

The observations at each time step k are formed by (2), as

$$\mathbf{y}_k = [\nabla \Delta P_{br,k}^{l1} \ \cdots \ \nabla \Delta P_{br,k}^{lM} \ \nabla \Delta \Phi_{br,k}^{l1} \ \cdots \ \nabla \Delta \Phi_{br,k}^{lM}]^\top, \quad (4)$$

yielding the corresponding measurement model

$$\mathbf{y}_k = \mathbf{h}(\mathbf{x}_k) + \mathbf{g}(\mathbf{n}_k) + \mathbf{e}_k, \quad (5a)$$

$$\mathbf{h}(\mathbf{x}_k) = [\nabla \Delta \rho_{br,k}^{l1} \ \cdots \ \nabla \Delta \rho_{br,k}^{lM} \ \nabla \Delta \rho_{br,k}^{l1} \ \cdots \ \nabla \Delta \rho_{br,k}^{lM}]^\top, \quad (5b)$$

$$\mathbf{g}(\mathbf{n}_k) = \lambda [0 \ \cdots \ 0 \ \mathbf{n}_k^\top]^\top, \quad (5c)$$

$$\mathbf{e}_k = [\nabla \Delta \epsilon_{br,k}^{l1} \ \cdots \ \nabla \Delta \epsilon_{br,k}^{lM} \ \nabla \Delta \eta_{br,k}^{l1} \ \cdots \ \nabla \Delta \eta_{br,k}^{lM}]^\top. \quad (5d)$$

For future reference and simplicity, we let $\mathbf{e}_k \sim \mathcal{N}(\mathbf{0}, \mathbf{R}_k)$.

As the estimator is to be used for receivers employed in various applications, we consider a generic motion model

$$\mathbf{x}_{k+1} = \mathbf{F}_k \mathbf{x}_k + \mathbf{B}_k \mathbf{w}_{\mathbf{x},k}, \quad (6)$$

where \mathbf{F}_k is the state-transition matrix and \mathbf{B}_k is the noise-transition matrix. In the numerical evaluation in Section VI, we use a constant-velocity (CV) model with state vector $\mathbf{x}_k = [\mathbf{p}_{r,k} \ \mathbf{v}_{r,k}]^\top \in \mathbb{R}^6$, where $\mathbf{p}_{r,k}$ and $\mathbf{v}_{r,k}$ are the receiver position and velocity respectively, but more complex models can be used. The CV model is then discretized using zero-order hold sampling with sampling period T_s [12], with

$$\mathbf{x}_{k+1} = \begin{bmatrix} \mathbf{I} & T_s \mathbf{I} \\ \mathbf{0} & \mathbf{I} \end{bmatrix} \mathbf{x}_k + \begin{bmatrix} \frac{T_s^2}{2} \mathbf{I} \\ T_s \mathbf{I} \end{bmatrix} \mathbf{w}_{\mathbf{x},k}, \quad (7)$$

with $\mathbf{w}_{\mathbf{x},k} \sim \mathcal{N}(\mathbf{0}, \mathbf{Q}_{\mathbf{x},k})$. In the next section, we address the problem of recursively estimating $p(\mathbf{x}_k, \mathbf{n}_k | \mathbf{y}_{0:k})$, for $\mathbf{x}_k \in \mathbb{R}^6$, $\mathbf{n}_k \in \mathbb{Z}^M$ given the measurements $\mathbf{y}_{0:k} \in \mathbb{R}^{2M}$ in (5).

III. THE BASELINE IMMEKF

In this section, we briefly outline the algorithm presented in [11], here referred to as the baseline integer mixture model Extended Kalman filter (IMMEKF), which we will augment with the optimal measurement projections in later sections. For additional details on the original algorithm, refer to [11].

A. Ambiguity prediction model

The estimation model consisting of (5) and (6) is nonlinear in the position due to the observation equations, but linear in the ambiguity vector. To reflect the uncertainty in the time evolution of the ambiguities, we assume that

$$\mathbf{n}_{k+1} = \mathbf{n}_k + \mathbf{w}_{\mathbf{n},k}, \quad \mathbf{w}_{\mathbf{n},k} \sim \mathcal{N}(\mathbf{0}, \mathbf{Q}_{\mathbf{n}}). \quad (8)$$

Using a random walk for the time evolution of the ambiguities is standard (c.f. [9], [14]). However, a key difference in [10] is that $\mathbf{Q}_{\mathbf{n}}$ is chosen large to a point where the measurements essentially determine the range of possible \mathbf{n}_k .

B. Bounding the Range of Ambiguities

The algorithm in [11] is based on estimating the ambiguities in a PF, bounding the possible range of the ambiguities and thereby permitting fixing of set of integer ambiguity hypotheses in (3). A bank of EKFs is then used, where the state-distribution in each EKF is constrained to a particular integer vector in the set of ambiguity hypotheses. To bound the range of ambiguities, the density $p(\mathbf{x}_k, \mathbf{n}_{0:k} | \mathbf{y}_{0:k})$ of state \mathbf{x}_k and ambiguity trajectory $\mathbf{n}_{0:k}$ is decomposed as

$$p(\mathbf{x}_k, \mathbf{n}_{0:k} | \mathbf{y}_{0:k}) = p(\mathbf{x}_k | \mathbf{n}_{0:k}, \mathbf{y}_{0:k}) p(\mathbf{n}_{0:k} | \mathbf{y}_{0:k}). \quad (9)$$

To resolve (9), $p(\mathbf{n}_{0:k} | \mathbf{y}_{0:k})$ is estimated with a PF using a set of N weighted particles, resulting in the approximation

$$p(\mathbf{n}_{0:k} | \mathbf{y}_{0:k}) \approx \sum_{i=1}^N q_k^i \delta(\mathbf{n}_{0:k}^i - \mathbf{n}_{0:k}). \quad (10)$$

In (10), $\delta(\cdot)$ is the Dirac delta mass and q_k^i is the associated weight for the i^{th} particle given the measurements $\mathbf{y}_{0:k}$.

Given the ambiguity set $\{\mathbf{n}_{0:k}^i\}_{i=1}^N$, a set of constrained EKFs are executed to determine the first term on the right-hand side of (9), with the Gaussian approximation

$$p(\mathbf{x}_k|\mathbf{n}_{0:k}, \mathbf{y}_{0:k}) \approx \mathcal{N}(\mathbf{x}_k; \hat{\mathbf{x}}_{k|k}(\mathbf{n}_{0:k}^i), \mathbf{P}_{k|k}(\mathbf{n}_{0:k}^i)), \quad (11)$$

for each particle. In (11), $\hat{\mathbf{x}}_{k|k}(\mathbf{n}_{0:k}^i)$ is the state estimate mean, constrained to the ambiguity trajectory $\mathbf{n}_{0:k}$, and $\mathbf{P}_{k|k}(\mathbf{n}_{0:k})$ is its associated covariance. For brevity, the dependence on the ambiguity trajectory is made implicit (i.e., $\mathbf{P}_{k|k}^i := \mathbf{P}_{k|k}(\mathbf{n}_{0:k}^i)$). The mean and covariance of the distribution in (11) is computed in an EKF update [19],

$$\hat{\mathbf{x}}_{k|k}^i = \hat{\mathbf{x}}_{k|k-1}^i + \mathbf{K}_k(\mathbf{y}_k - \hat{\mathbf{y}}_{k|k-1}^i), \quad (12a)$$

$$\mathbf{P}_{k|k}^i = \mathbf{P}_{k|k-1}^i - \mathbf{K}_k \mathbf{H}_k \mathbf{P}_{k|k-1}^i, \quad (12b)$$

$$\hat{\mathbf{y}}_{k|k-1}^i = \mathbf{h}(\hat{\mathbf{x}}_{k|k-1}^i) + \mathbf{g}(\mathbf{n}_{0:k}^i), \quad (12c)$$

$$\mathbf{S}_k = \mathbf{H}_k \mathbf{P}_{k|k-1}^i \mathbf{H}_k^\top + \mathbf{R}_k, \quad (12d)$$

$$\mathbf{K}_k = \mathbf{P}_{k|k-1}^i \mathbf{H}_k^\top \mathbf{S}_k^{-1}, \quad (12e)$$

$$\mathbf{H}_k = (\partial \mathbf{h}(\mathbf{x})) / (\partial \mathbf{x})|_{\mathbf{x}=\hat{\mathbf{x}}_{k|k-1}^i}, \quad (12f)$$

and the one-step prediction of the mean and covariance are

$$\hat{\mathbf{x}}_{k|k-1}^i = \mathbf{F}_{k-1} \hat{\mathbf{x}}_{k-1|k-1}^i, \quad (13a)$$

$$\mathbf{P}_{k|k-1}^i = \mathbf{F}_{k-1} \mathbf{P}_{k-1|k-1}^i \mathbf{F}_{k-1}^\top + \mathbf{Q}_{\mathbf{x},k-1}. \quad (13b)$$

As in [11], the weight update of the PF is given by

$$q_k^i = \frac{p(\mathbf{y}_k|\mathbf{n}_k, \mathbf{y}_{0:k-1})p(\mathbf{n}_k|\mathbf{n}_{k-1}^i)}{\pi(\mathbf{n}_k|\mathbf{n}_{k-1}^i, \mathbf{y}_{0:k})} q_{k-1}^i, \quad (14)$$

where the proposal density is chosen as,

$$\pi(\mathbf{n}_k|\mathbf{n}_{k-1}^i, \mathbf{y}_{0:k}) = p(\mathbf{n}_k|\mathbf{n}_{k-1}^i, \mathbf{y}_{0:k}), \quad (15)$$

and inserting (15) into (14) leads to the recursive update

$$q_k^i \propto p(\mathbf{y}_k|\mathbf{n}_{k-1}^i, \mathbf{y}_{0:k-1}) q_{k-1}^i. \quad (16)$$

The proposal (15) is optimal in the sense that it minimizes the effect of the sampling on the weights, that is, the weights will be unaffected by \mathbf{n}_k^i , whereas other alternatives add variance among the weights [12]. It is generally difficult to sample from (15). However, the observation equation (5) is linear and Gaussian in the ambiguity vector \mathbf{n}_k , which is one of the few cases where exact sampling is possible [20], [21]. In this case, the optimal proposal (15) for a marginalized PF is

$$p(\mathbf{n}_k|\mathbf{n}_{k-1}^i, \mathbf{y}_{0:k}) = \mathcal{N}(\mathbf{n}_k; \hat{\mathbf{n}}_k^i, \mathbf{\Sigma}_k^i), \quad (17a)$$

$$\hat{\mathbf{n}}_k^i = \hat{\mathbf{n}}_{k-1}^i + \mathbf{K}_k(\mathbf{y}_k - \hat{\mathbf{y}}_{k|k-1}^i), \quad (17b)$$

$$\mathbf{K}_k = \mathbf{Q}_n \mathbf{G}_k^\top (\mathbf{G}_k \mathbf{Q}_n \mathbf{G}_k^\top + \mathbf{S}_k^i)^{-1}, \quad (17c)$$

$$\mathbf{\Sigma}_k^i = (\mathbf{Q}_n^{-1} + \mathbf{G}_k^\top (\mathbf{S}_k^i)^{-1} \mathbf{G}_k)^{-1}, \quad (17d)$$

$$\mathbf{G}_k = (\partial \mathbf{g}(\mathbf{n})) / (\partial \mathbf{n}). \quad (17e)$$

where \mathbf{S}_k^i is obtained from (12d), conditioned on the i^{th} ambiguity trajectory. With the optimal proposal (17a), the likelihood for the weight update in (16) is

$$p(\mathbf{y}_k|\mathbf{n}_{k-1}^i, \mathbf{y}_{0:k-1}) \approx \mathcal{N}(\mathbf{y}_k; \hat{\mathbf{y}}_{k|k-1}^i, \mathbf{Q}_n + \mathbf{S}_k^i), \quad (18a)$$

where $\hat{\mathbf{y}}_{k|k-1}^i$ is obtained from (12c). Note that although the optimal proposal (17a) and therefore also the likelihood (18a)

are linear in the ambiguities, the covariance \mathbf{S}_k^i is obtained from the EKF recursion, which is approximate.

The generated ambiguities are real-valued when using the optimal proposal (17), and after re-sampling (10), we obtain

$$p(\mathbf{n}_k|\mathbf{y}_{0:k}) \approx \hat{p}(\mathbf{n}_k|\mathbf{y}_{0:k}) = \frac{1}{N} \sum_{i=1}^N \delta(\mathbf{n}_k^i - \mathbf{n}_k). \quad (19)$$

To get a measure of the tails of (19) for a finite number of particles, the discrete representation is converted to a continuous density using a kernel density smoother [22],

$$\hat{p}_K(\mathbf{n}_k|\mathbf{y}_{0:k}) = \frac{1}{N} \sum_{i=1}^N K_h(\mathbf{n}_k^i - \mathbf{n}_k), \quad (20)$$

where $K_h(\cdot)$ is the kernel density and h is the bandwidth. We truncate (20), resulting in the continuous truncated density $\hat{p}_{K,\text{tr}}(\mathbf{n}_k|\mathbf{y}_{0:k})$. Based on $\hat{p}_{K,\text{tr}}(\mathbf{n}_k|\mathbf{y}_{0:k})$ we fix the ambiguities, which gives a finite set \mathcal{S} of N_S possible integer vectors $\{\mathbf{n}_1^i\}_{i=1}^{N_S}$ contained in the support of $\hat{p}_{K,\text{tr}}$, that is,

$$\mathcal{S} = \{\mathbf{n}_1 \in \mathbb{Z}^M : \hat{p}_{K,\text{tr}}(\mathbf{n}_1|\mathbf{y}_{0:k}) > 0\}. \quad (21)$$

The weight update (16) of the PF and (19)–(21) do not need to be performed at every time step. In practice, we only execute (16), (18a), (19)–(21) if a significant difference is detected between the float ambiguity hypotheses on two consecutive time-steps, or if a cycle slip is detected, warranting a re-initialization of the ambiguity hypotheses in \mathcal{S} .

C. Ambiguity Resolution by Mixture Kalman Filter

Provided the N_S possible integer vectors in (21), N_S EKFs are executed in parallel to find the state vectors $\hat{\mathbf{x}}_k^{\text{KF},i}$, where each EKF is conditioned on a unique integer ambiguity vector $\mathbf{n}_1^i \in \mathcal{S}$. The state posterior is expressed using the law of total probability as a Gaussian mixture of N_S components,

$$p(\mathbf{x}_k^{\text{KF}}|\mathbf{y}_{0:k}) = \sum_{i=1}^{N_S} \omega_k^i \mathcal{N}(\mathbf{x}_k^{\text{KF}}|\hat{\mathbf{x}}_{k|k}^{\text{KF},i}, \mathbf{P}_{k|k}^i), \quad (22)$$

where $\omega_k^i = p(\mathbf{n}_1^i|\mathbf{y}_{0:k})$ is the posterior probability of \mathbf{n}_1^i . The recursions for $\hat{\mathbf{x}}_{k|k}^{\text{KF},i}$, $\mathbf{P}_{k|k}^i$ are in (12) with \mathbf{n}_k^i replaced with \mathbf{n}_1^i . The weights ω_k^i can be computed recursively,

$$\omega_k^i = p(\mathbf{n}_1^i|\mathbf{y}_{0:k}) \propto \omega_{k-1}^i \mathcal{N}(\mathbf{y}_k|\hat{\mathbf{y}}_{k|k-1}^i, \mathbf{S}_k^i), \quad (23)$$

where the prediction mean and covariance $\hat{\mathbf{y}}_{k|k-1}^i$, \mathbf{S}_k^i are given from the associated EKF. From (23), we use the maximum-likelihood (ML) estimate to resolve the ambiguity, and visualize the state estimate in terms of the first two moments of the EKF bank at time-step k [19], as

$$\hat{\mathbf{x}}_{k|k}^{\text{MV}} = \sum_{i=1}^{N_S} \omega_k^i \hat{\mathbf{x}}_{k|k}^{\text{KF},i}, \quad \mathbf{n}_k^{\text{ML}} = \arg \max_{\mathbf{n}_1 \in \mathcal{S}} \omega_k^i, \quad (24)$$

$$\mathbf{P}_{k|k}^{\text{MV}} = \sum_{i=1}^{N_S} \omega_k^i \left(\mathbf{P}_{k|k}^i + (\hat{\mathbf{x}}_{k|k}^{\text{KF},i} - \hat{\mathbf{x}}_{k|k}^{\text{MV}})(\hat{\mathbf{x}}_{k|k}^{\text{KF},i} - \hat{\mathbf{x}}_{k|k}^{\text{MV}})^\top \right),$$

but the underlying distribution of the bank is likely to be multimodal. This is the baseline algorithm presented in [11], which we will improve in terms computational tractability, before introducing the optimal measurement projections.

D. Improving the algorithm's numerical robustness

Considering the algorithm in [11] with the ambiguity sampling in (17), the measurement equation in (5) yields $(\mathbf{G}_k^\top \mathbf{G}_k)^{-1} = \lambda^{-2} \mathbf{I}$. Hence, we can simplify (17) significantly. Using $\mathbf{S}_k^i, \mathbf{Q}_n \succ 0$ and the Woodbury identity [23],

$$p(\mathbf{n}_k | \mathbf{n}_{k-1}^i, \mathbf{y}_{0:k}) = \mathcal{N}(\mathbf{n}_k; \hat{\mathbf{n}}_k^i, \lambda^{-2} \mathbf{K}_k \mathbf{S}_k^i \mathbf{G}_k), \quad (25a)$$

$$\hat{\mathbf{n}}_k^i = \hat{\mathbf{n}}_{k-1}^i + \mathbf{K}(\mathbf{y}_k - \hat{\mathbf{y}}_k^i), \quad (25b)$$

$$\mathbf{K}_k = \mathbf{Q}_n \mathbf{G}_k^\top (\mathbf{G}_k \mathbf{Q}_n \mathbf{G}_k^\top + \mathbf{S}_k^i)^{-1}. \quad (25c)$$

This both improves the numerical robustness of the filter and reduces the computational complexity by virtue of removing two of the three matrix inversions in (17). We refer to a filter using the recursions in previous sections, with the sampling of ambiguities in (25) replacing that of (17), as the IMMEKF.

IV. OPTIMAL MEASUREMENT PROJECTIONS

The main computational bottleneck of the IMMEKF stems from the large number of hypotheses that need to be entertained at the moment of reinitializing the KF bank. To illustrate this, assume that we have $M = 10$, with approximately five unique integers in the support of the kernel density estimate. This would amount to a total of $N_S = 5^M \approx 10^7$ EKFs, which need to be run in parallel at the moment of re-initialization. The number of hypotheses quickly decrease by virtue of the measurement updates and re-sampling, but the need for performing N_S such updates with $\mathbf{y}_k \in \mathbb{R}^{2M}$ and inverting $\mathbf{S}_k \in \mathbb{R}^{2M \times 2M}$ is responsible for the bulk of the computational time of the IMMEKF. In this section, we address this problem by first projecting \mathbf{y}_k before evaluating the EKF measurement update in (12).

A. Formulating the optimization program

We seek a projected measurement vector $\tilde{\mathbf{y}}_k = \Psi_k(\mathbf{y}_k)$, where $\Psi_k : \mathbb{R}^{2M} \rightarrow \mathbb{R}^{\tilde{M}}$ for a some $\tilde{M} \leq 2M$, such that a maximal amount of information is retained in the projected measurements. Since the measurement equation (5) only depends on the positional states, we will instead refer to it by a function $\mathbf{h}_p : \mathbb{R}^3 \rightarrow \mathbb{R}^{2M}$, such that $\mathbf{h}_p(\mathbf{p}_{r,k}) = \mathbf{h}(\mathbf{x}_{r,k})$. For clarity, we will temporarily drop the time-indexation in the developments below. To quantify the quality of a projection, we consider the local positional MSE CRB. Take the position to be the parameter vector θ , let $\mathbf{R} = \text{Cov}(\mathbf{e})$ in (5), and consider the density function of the measurement

$$p(\mathbf{y}; \theta) = \mathcal{N}(\mathbf{y}; \mathbf{h}_p(\theta), \mathbf{R}). \quad (26)$$

For any unbiased estimate $\hat{\theta}$ of θ given samples of (26) [13],

$$\mathbb{E}[\|\theta - \hat{\theta}\|_2^2] = \text{Tr}(\mathbb{E}[(\theta - \hat{\theta})(\theta - \hat{\theta})^\top]) > \text{Tr}(\mathcal{I}(\theta; \mathbf{y})^{-1}), \quad (27)$$

with $\mathcal{I}(\theta; \mathbf{y})$ denoting the FIM of any unbiased estimate $\hat{\theta}$ of θ given a sample from $p(\mathbf{y}; \theta)$. Since the measurement noise in (5) is zero-mean and Gaussian, and with a covariance $\mathbf{R} \succ 0$ independent of θ , the FIM for a specific $\theta = \mathbf{p}^*$ is

$$\mathcal{I}(\theta; \mathbf{y}) = \mathbf{H}_p^\top \mathbf{R}^{-1} \mathbf{H}_p, \quad \mathbf{H}_p = (\partial \mathbf{h}_p(\theta)) / (\partial \theta)|_{\theta=\mathbf{p}^*} \quad (28)$$

Now, if we were to project the measurements into an \tilde{M} -dimensional subspace $\tilde{\mathbf{y}} = \Psi \mathbf{y}$, and constrain Ψ to be a linear map, we get the pdf of the projected measurements as

$$p(\tilde{\mathbf{y}}; \theta) = \mathcal{N}(\tilde{\mathbf{y}}; \Psi \mathbf{h}_p(\theta), \Psi \mathbf{R} \Psi^\top). \quad (29)$$

With the projected measurements, the FIM is

$$\mathcal{I}(\theta; \tilde{\mathbf{y}}) = (\Psi \mathbf{H}_p)^\top (\Psi \mathbf{R} \Psi^\top)^{-1} \Psi \mathbf{H}_p. \quad (30)$$

Consequently, the problem of finding the optimal projection operator that minimizes CRB of the positional MSE at a specific receiver position $\theta = \mathbf{p}^*$ for a desired projected measurement dimension $\tilde{M} \leq 2M$, can be formulated as

$$\min J(\Psi) \text{ over } \Psi \in \mathbb{R}^{\tilde{M} \times M} \quad (31)$$

with a matrix-valued objective function $J : \mathbb{R}^{\tilde{M} \times M} \rightarrow \mathbb{R}$,

$$J(\Psi) = \text{Tr}([\Psi \mathbf{H}_p]^\top (\Psi \mathbf{R} \Psi^\top)^{-1} \Psi \mathbf{H}_p)^{-1}. \quad (32)$$

Note that the cost in (32) is scale invariant in the sense that $J(\alpha \Psi) = J(\Psi)$ for all $\alpha > 0$, meaning that we are free to normalize the projection operator. The program (31) is non-convex and can only be solved to a local optimum, but the quality of a solution can easily be determined.

Remark 1: If $J(\Psi) \rightarrow J(\mathbf{I})$, then we will have the same positional MSE CRB when using the projected and original measurements in estimating θ . Furthermore, if we find an estimator with MSE-performance close to the CRB, the ratio $J(\Psi)/J(\mathbf{I}) \geq 1$ is the relative decrease in MSE performance when filtering with $\tilde{\mathbf{y}} = \Psi \mathbf{y}$ as compared to using \mathbf{y} .

Remark 2: In evaluating the cost in (32), \mathbf{H}_p is evaluated using a first-order Taylor expansion about $\theta = \mathbf{p}^*$. The numerically evaluated CRBs are then approximate, but motivated by the fact that \mathbf{h}_p is approximately linear in \mathbf{p} given the large distances between satellites and receivers. To illustrate this, take a perturbation $\delta \in \mathbb{R}^3$, with $\|\delta\|_2 \leq D$. Since the satellites orbit the Earth at $\rho^j \approx 3 \cdot 10^7$ [m], it is clear that $\|\mathbf{p}^j + \delta\|_2 \approx \|\mathbf{p}^j\|_2 = \rho^j$. Taking a single element of the function \mathbf{h}_p involving satellites i and j as $h_p^{ij}(\theta)$,

$$\frac{\partial h_p^{ij}(\theta + \delta)}{\partial \theta} \approx \frac{\partial h_p^{ij}(\theta)}{\partial \theta} + \frac{(\rho_r^i - \rho_r^j)}{\rho_r^i \rho_r^j} o(\|\delta\|). \quad (33)$$

Since the maximum possible difference $(\rho_r^i - \rho_r^j)$ is the Earth diameter at $12 \cdot 10^6$, the perturbation δ will not change any element of the positional Jacobian more than by a value of approximately $(4D/3) \cdot 10^{-8}$, motivating the use of the first-order Taylor expansions for evaluating the CRB in Remark 2.

B. Solving the optimization program

The optimization problem posed in (32) has some beneficial structure. To solve it efficiently by gradient-based methods, we give the gradient of $J(\Psi)$ in Proposition 1.

Proposition 1: The partial derivative of the CRB in (32) when using projected measurements $\tilde{\mathbf{y}} = \Psi \mathbf{y}$ at $\theta = \mathbf{p}^*$, is

$$\frac{\partial \text{Tr}(\mathcal{I}(\theta; \tilde{\mathbf{y}})^{-1})}{\partial \Psi} = -2\mathbf{U} \mathbf{Q} \mathbf{\Lambda}^{-2} \mathbf{Q}^\top \mathbf{V}^\top, \quad (34)$$

where

$$\mathbf{Y} = \mathbf{H}_p^\top \Psi^\top (\Psi \mathbf{R} \Psi^\top)^{-1} \Psi \mathbf{H}_p, \quad (35a)$$

$$\mathbf{U} = (\Psi \mathbf{R} \Psi^\top)^{-1} \Psi \mathbf{H}_p, \quad (35b)$$

$$\mathbf{V} = \mathbf{H}_p - \mathbf{R} \Psi^\top \mathbf{U}, \quad (35c)$$

and $\mathbf{Y} = \mathbf{Q} \Lambda \mathbf{Q}^\top$ and the Jacobian matrix \mathbf{H}_p given in (28).

Remark 3: The partial derivative exists at all times provided $\text{rank}(\Psi) \geq 3$, which requires $\tilde{M} \geq 3$, and can be ensured by adding a rank constraint to the optimization program. However, for any practical implementation, adding a line-search to the gradient descent allows the selection of an element of a $\Psi \in \mathbb{R}^{\tilde{M} \times 2M}$ that meets this condition.

In the context of the estimation problem, we give a simple gradient-descent algorithm that exploits Proposition 1. With a noise covariance \mathbf{R}_k and positional Jacobian matrix $\mathbf{H}_{p,k}$ at a time-step k , and denote the gradient-descent iterations by the sub-index n . Taking a random initialization $\Psi_{k,n} \in \mathbb{R}^{\tilde{M} \times 2M}$ at $n = -1$ satisfying the rank constraint,

$$\Psi_{k,n} = \Psi_{k,n-1} + 2\gamma \mathbf{U}_n \mathbf{Q}_n \Lambda_n^{-2} \mathbf{Q}_n^\top \mathbf{V}_n^\top, \quad (36a)$$

$$[\Lambda_n, \mathbf{Q}_n] = \text{eig}(\mathbf{Y}_n), \quad (36b)$$

$$\mathbf{Y}_n = \mathbf{H}_{p,k}^\top \Psi_{k,n-1}^\top \mathbf{U}_n, \quad (36c)$$

$$\mathbf{V}_n = \mathbf{H}_{p,k} - \mathbf{R}_k \Psi_{k,n-1}^\top \mathbf{U}_n, \quad (36d)$$

$$\mathbf{U}_n = (\Psi_{k,n-1} \mathbf{R}_k \Psi_{k,n-1}^\top)^{-1} \Psi_{k,n-1} \mathbf{H}_{p,k}, \quad (36e)$$

$$\mathbf{H}_p = (\partial \mathbf{h}_p(\boldsymbol{\theta})) / (\partial \boldsymbol{\theta})|_{\boldsymbol{\theta}=\mathbf{p}_k^*}, \quad (36f)$$

ensures convergence of $\Psi_{k,n}$ to a local optimum for large n if γ is found by a line-search. We will refer to the locally optimal projection at k as $\Psi_{k,\infty}$, but have yet to define the position $\boldsymbol{\theta} = \mathbf{p}^*$ at which the CRB in (32) is to be evaluated.

V. DEVELOPMENT OF A PROJECTIVE IMMEKF

The particles in the IMMEKF typically reside within meters of each other in terms of the positional states, compared to the tens of thousands of kilometers between the receiver and the satellites. Consequently, the positional Jacobian $\mathbf{H}_{p,k}$ in (36) will not change significantly among the particles in the EKF bank. This implies a small change in optimization cost function (32), were the FIM to be re-computed for all the unique positions in the EKF bank. Consequently, we will use the same projection operator in all of the particles, optimized with respect to the weighted mean position, $\mathbf{p}_k^* = \hat{\mathbf{p}}_{k|k}^{MV}$, as the positional subset of $\hat{\mathbf{x}}_{k|k}^{MV}$ computed in (24).

A. Consequences for the IMMEKF

If a locally optimal operator $\Psi_{k,\infty}$ can be computed at each time-step by (36), and if this is used to evaluate the projected measurements, we get a measurement model

$$\tilde{\mathbf{y}}_k = \Psi_{k,\infty} \mathbf{y}_k = \Psi_{k,\infty} (\mathbf{h}(\mathbf{x}_k) + \mathbf{g}(\mathbf{n}_k) + \mathbf{e}_k). \quad (37)$$

Utilizing (29), we can evaluate the projected measurement and its covariance, which will be the same for all particles,

$$\tilde{\mathbf{y}}_k = \Psi_{k,\infty} \mathbf{y}_k, \quad \tilde{\mathbf{R}}_k = \Psi_{k,\infty} \mathbf{R}_k \Psi_{k,\infty}^\top, \quad (38)$$

and the Kalman filter updates, now using (37), takes the form

$$\hat{\mathbf{x}}_{k|k}^i = \hat{\mathbf{x}}_{k|k-1}^i + \mathbf{K}_k (\tilde{\mathbf{y}}_k - \hat{\mathbf{y}}_{k|k-1}^i), \quad (39a)$$

$$\mathbf{P}_{k|k}^i = \mathbf{P}_{k|k-1}^i - \tilde{\mathbf{K}}_k \tilde{\mathbf{H}}_k \mathbf{P}_{k|k-1}^i, \quad (39b)$$

$$\hat{\mathbf{y}}_{k|k-1}^i = \Psi_{k,\infty} [\mathbf{h}(\hat{\mathbf{x}}_{k|k-1}^i) + \mathbf{g}(\mathbf{n}_k^i)], \quad (39c)$$

$$\tilde{\mathbf{S}}_k = \tilde{\mathbf{H}}_k \mathbf{P}_{k|k-1} \tilde{\mathbf{H}}_k^\top + \tilde{\mathbf{R}}_k, \quad (39d)$$

$$\tilde{\mathbf{K}}_k = \mathbf{P}_{k|k-1} \tilde{\mathbf{H}}_k^\top \tilde{\mathbf{S}}_k^{-1}, \quad (39e)$$

$$\tilde{\mathbf{H}}_k = \Psi_{k,\infty} (\partial \mathbf{h}(\mathbf{x})) / (\partial \mathbf{x})|_{\mathbf{x}=\hat{\mathbf{x}}_{k|k-1}^i}. \quad (39f)$$

We refer to a filter using the online adaption of the projection operator in (36) with the Kalman filter update in (39) as the P-IMMEKF. This is summarized in Algorithm 1.

B. Consequences for computational complexity

To get a rough idea of the computational complexity, take the inversion of a dense rectangular $M \times M$ -matrix to be $O(M^3)$, the computation of its eigen-decomposition to also be $O(M^3)$, and disregard the smaller matrix products and additions involved in the EKF update. The computational complexity of the filter bank re-initialization will be approximately $O(N_S(2M)^3)$. On the other hand, if we instead use the projected measurements with N_I iterations per epoch, we will have $O(N_S \tilde{M}^3 + N_I \tilde{M}^3)$. However, it remains to see how small we can choose \tilde{M} , so as not to significantly increase the CRB ratio $J(\Psi_{k,\infty})/J(\mathbf{I})$. For small \tilde{M} , and if $N_I \ll N_S$, it will clearly be computationally favorable to use the optimal projection in the EKF measurement updates.

Algorithm 1 The P-IMMEKF with optimal projections

- 1: **Initialize:** Draw $\Psi_{0,0} \sim \mathcal{U}([-1, 1]^{\tilde{M} \times 2M})$, $\{\mathbf{n}_{-1}^i\}_{i=1}^N \sim p_0(\mathbf{n}_0)$, $\{\hat{\mathbf{x}}_{0|-1}^i\}_{i=1}^N \sim p_0(\mathbf{x}_0)$, $\{\mathbf{P}_{0|-1}^i\}_{i=1}^N = \mathbf{P}_0$, $\{\hat{\mathbf{x}}_0^{\text{KF},i}\}_{i=1}^{N_S} \sim p_0(\mathbf{x}_0)$, $\{\mathbf{P}_{0|-1}^{\text{KF},i}\}_{i=1}^{N_S} = \mathbf{P}_0$, $\{w_{-1}^i\}_{i=1}^N = 1/N$.
 - 2: **for** $n = 1$ **to** N_I^0 **do**
 - 3: Update $\Psi_{0,n}$ using the recursions in (36).
 - 4: **for** $k = 0$ **to** T **do**
 - 5: **for** $i = 1$ **to** N **do**
 - 6: Update $\{\hat{\mathbf{x}}_{k|k-1}^i, \mathbf{P}_{k|k-1}^i\}$ using (13).
 - 7: Generate $\mathbf{n}_k^i \sim p(\mathbf{n}_k | \mathbf{n}_{k-1}^i, \mathbf{y}_{0:k})$ from (25).
 - 8: **if** reinitialize **then**
 - 9: Compute $\tilde{\mathbf{y}}_k$ and $\tilde{\mathbf{R}}_k$ using (38).
 - 10: **for** $i = 1$ **to** N **do**
 - 11: Update $\{\hat{\mathbf{x}}_{k|k}^i, \mathbf{P}_{k|k}^i\}$ from (39).
 - 12: Update q_k^i using (16) and (18a).
 - 13: Compute $\hat{p}_K(\mathbf{n}_k | \mathbf{y}_{0:k})$ using (20).
 - 14: Determine $\{\mathbf{n}_k^i\}_{i=1}^{N_S}$ using (21).
 - 15: Initialize $\{\hat{\mathbf{x}}_{k|k-1}^{\text{KF},i}, \mathbf{P}_{k|k-1}^{\text{KF},i}\}_{i=1}^{N_S}$.
 - 16: **else**
 - 17: Update $\{\hat{\mathbf{x}}_{k|k-1}^{\text{KF},i}, \mathbf{P}_{k|k-1}^{\text{KF},i}\}_{i=1}^{N_S}$ using (13).
 - 18: Compute $\tilde{\mathbf{y}}_k$ and $\tilde{\mathbf{R}}_k$ using (38).
 - 19: **for** $i = 1$ **to** N_S **do**
 - 20: Update $\{\hat{\mathbf{x}}_{k|k}^{\text{KF},i}, \mathbf{P}_{k|k}^{\text{KF},i}\}$ using (39).
 - 21: Update weight ω_k^i using (23).
 - 22: Compute $\{\mathbf{n}_k^{\text{ML}}, \hat{\mathbf{x}}_{k|k}^{\text{MV}}, \mathbf{P}_{k|k}^{\text{MV}}\}$ using (24).
 - 23: Set $\Psi_{k,0} = \Psi_{k-1,\infty}$
 - 24: **for** $n = 1$ **to** N_I **do**
 - 25: Update $\Psi_{k,n}$ using the recursions in (36).
 - 26: **for** $i = 1$ **to** N **do**
 - 27: Draw index $J(i)$ with probability $\omega_k^{J(i)}$.
 - 28: Set $\{\mathbf{n}_k^i, \hat{\mathbf{x}}_{k|k}^i, \mathbf{P}_{k|k}^i\}_{i=1}^N = \{\mathbf{n}_k^l, \hat{\mathbf{x}}_{k|k}^{\text{KF},l}, \mathbf{P}_{k|k}^{\text{KF},l}\}_{l=J(1)}^{J(N)}$.
-

VI. NUMERICAL RESULTS

To evaluate the theory on optimal measurement projections and its utility for the marginalized PF approaches in GNSS positioning, we (i) show the soundness of the optimization scheme proposed in (36); (ii) give a simulation example showing the difference in executing the IMMEKF and the P-IMMEKF on synthetic data; and (iii) compute and compare the MSE of the positional estimate in a set of Monte Carlo (MC) runs, and their mean computational times.

A. Problem Setup

Throughout the numerical examples, we generate a set of positions uniformly $\bar{\mathbf{p}}^a \sim \mathcal{U}((0, 1]^3)$, and normalize these such that $\mathbf{p}^a = \rho^a \|\bar{\mathbf{p}}^a\|_2^{-1} \bar{\mathbf{p}}^a$ for some radius r^a . For the satellites, we let $\rho^j = 3 \cdot 10^7$ corresponding to GPS satellites, for the static base station we let $\rho^b = 6.3 \cdot 10^6$, and the true initial position of the receiver is similarly initialized at $\rho^r = 6.3 \cdot 10^6$, corresponding to positions somewhere on the Earth's surface. The receiver is then driven by a random walk in the velocity states, governed by the covariance $\mathbf{Q}_{x,k} = 0.1\mathbf{I}$. The true ambiguities used to generate the synthetic measurements are all initialized at a random integer in the set $\mathbf{n}_0 \in \mathcal{U}([-200, 200]^M)$, and every integer will change to some other value on this interval exactly once at a random time. The simulation is executed at a time-step of $h = 0.1$ [s] over a total of $T = 1000$ time steps. The measurement noise is zero mean and uncorrelated with $\epsilon_k^i \sim \mathcal{N}(0, 0.5^2)$ and $\eta_k^i \sim \mathcal{N}(0, 0.01^2)$ for all time steps k , and $M = 10$ pairs of code and phase measurements are used with a carrier wavelength $\lambda = 0.2$ [m], corresponding to the L_1 band. For the estimators, the process noise in the ambiguities are $\mathbf{Q}_{\mathbf{n},k} = 10\mathbf{I}$ and the filters use $N = 1000$ particles in the mixture model, using the heuristics in [10] to reinitialize the filters at cycle slips. For the projection optimization, we will use the smallest possible dimension, $\tilde{M} = 3$, that the theory in Section IV permits and a single gradient descent iteration, $N_I = 1$, per time-step. In our experience, the warm-started optimization scheme requires very few iterations per time-step, but this could be increased, to trade MSE-performance for computational time.

B. Validation of the projection optimization

To illustrate the projection optimization, we let $\tilde{M} = 3$ and randomize 20 unique problem setups from Section VI-A, along with 20 random initial projection operators from the uniform distribution $\Psi_{k,0} \sim \mathcal{U}([-1, 1]^{\tilde{M} \times 2M})$, and plot the cost $J(\Psi_{k,n})/J(\mathbf{I})$ as a function of the iteration number n , using the gradient descent iterations in (36). The result is shown in Figure 1, and indicates that regardless of initialization, we converge to something close to $J(\Psi_{k,n})/J(\mathbf{I}) = 1$.

C. Filter performance

In the next example, we show the filter performance of the IMMEKF and the P-IMMEKF when run on the exact same measurement data, with the exact same state initialization. In the IMMEKF, one gradient descent iteration is done per tune step, and before initializing the filter, $N_I = 10^5$ gradient

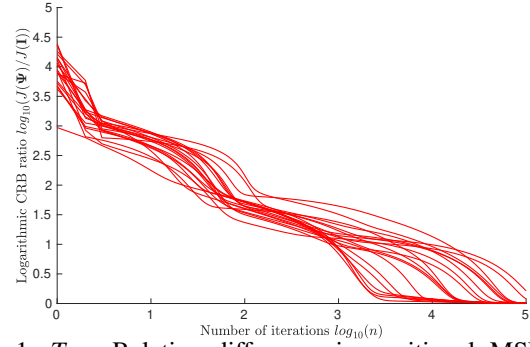


Fig. 1: *Top*: Relative difference in positional MSE CRB when using projected and un-projected measurements, $J(\Psi_{k,n})/J(\mathbf{I})$, as a function of n for 20 random initializations of $\Psi_{k,0}$, with $\gamma = 0.01$, $\tilde{M} = 3$ and $M = 10$.

descent iterations are done. Figure 2 shows the difference between $J(\Psi_{k,\infty})$ and $J(\mathbf{I})$ in time, Figure 3 and Figure 4 show the state estimates of the original IMMEKF (blue), the P-IMMEKF (red) and the true state trajectory (black) for the minimum variance state and the ambiguity estimates, respectively. Due to the very small gap in the projection ratio plot (see Figure 2), we should expect a very small difference between the filter performance in terms of positional MSE. The performance of the filters are extremely similar, despite the projected version using significantly less computational resources. To qualitatively compare their MSE performance, we next present a MC simulation study.

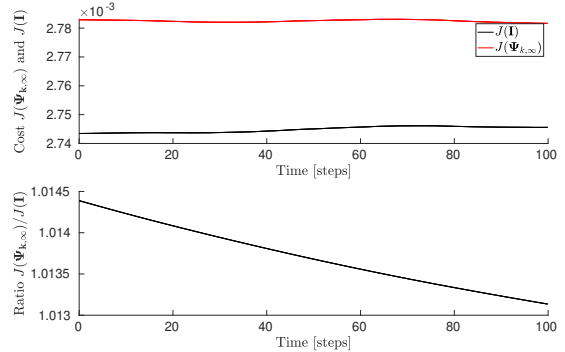


Fig. 2: *Top*: The locally optimal $\Psi_{k,\infty}$, in terms of $J(\Psi_{k,\infty})$ (red) compared to $J(\mathbf{I})$ (black) as a function of time [s] into the simulation. *Bottom*: The ratio $J(\Psi_{k,\infty})/J(\mathbf{I})$ in time.

D. Filter MSE-comparison

To further verify the theory and compare the two filters, 10^2 MC runs were executed on random problem initializations with the IMMEKF and the P-IMMEKF respectively, with the positional RMSE of the two filters depicted in Figure 5. As expected by the previous example of the CRB-optimization, the IMMEKF performs marginally better than the P-IMMEKF which uses the projected measurements, this is most clearly visible in the RMSE of $\hat{p}_{3r,k}$. The difference is insignificant, as one would expect since the CRBs only differ by 1% in Figure 2, but the computational efficiency of the projected filters is significantly better, with the mean computational time of the P-IMMEKF being 291.97 [s], compared to the mean computational time of 596.5 [s] of

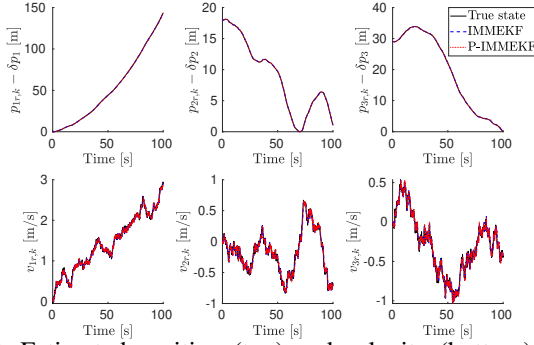


Fig. 3: Estimated position (top) and velocity (bottom) with the IMMEKF (blue), the P-IMMEKF (red) and ground truth (black), at a positional offset $\delta \mathbf{p} \approx [3.6 \ 3.5 \ 3.6]^T \cdot 10^6$.

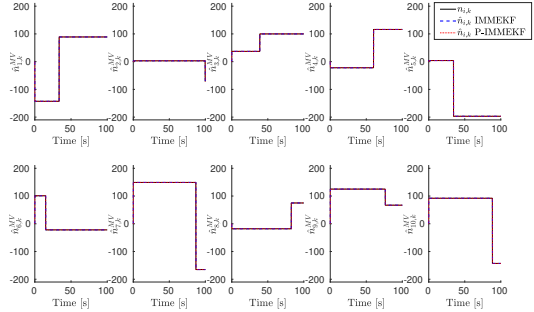


Fig. 4: Integer ambiguity estimates with the IMMEKF (blue), the P-IMMEKF (red) and the ground truth (black) from one sample of the 10^2 MC runs.

the IMMEKF. Note that this is the mean computational time running the filters over the entire data set in an un-optimized Matlab implementation, with many more cycle slips per time unit than what is typically present in real data.

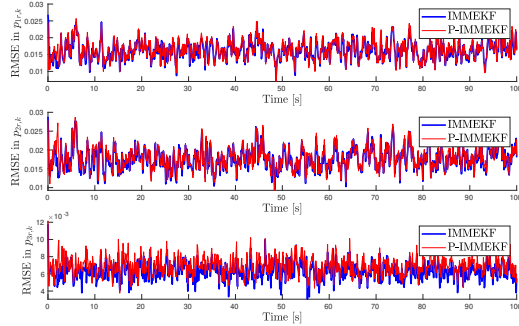


Fig. 5: RMSE of the positional state estimates with the IMMEKF (blue) and P-IMMEKF (red) from 10^2 MC runs.

VII. CONCLUSION

We have considered the marginalized PF approach in [10] for GNSS positioning known as the IMMEKF, and extended the algorithm to reduce the computational complexity of the ambiguity sampling, which can be crucial in implementations on consumer-grade GNSS receivers. To reduce computation further, we developed a framework for computing measurement subspaces in which the positional information of the acquired measurements is retained. As shown in Section VI-B, it is possible to compress a measurement vector $\mathbf{y} \in \mathbb{R}^{2M}$

into a projection $\tilde{\mathbf{y}} \in \mathbb{R}^{\tilde{M}}$ with $\tilde{M} = 3$, with minimal degradation to MSE-performance. Combined with the assumption that the positional Jacobian of the measurement equation varies little among the particles in the EKF bank, as shown in (32), we presented the P-IMMEKF. In this filter, a single projection operator is recursively updated and applied in all EKF updates. We noted a significant speed-up of the algorithm, and validated the theoretical conclusions by empirically computing the positional MSE in a MC study.

REFERENCES

- [1] B. Hofmann-Wellenhof, H. Lichtenegger, and J. Collins, *Global Positioning System: theory and practice*. Springer-Verlag, 1997.
- [2] P. Teunissen, "Theory of carrier phase ambiguity resolution," *Wuhan University Journal of Natural Sciences*, vol. 8, no. 2, p. 471, 2003.
- [3] S. Zhao, X. Cui, F. Guan, and M. Lu, "A Kalman filter-based short baseline RTK algorithm for single-frequency combination of GPS and BDS," *Sensors*, vol. 14, no. 8, pp. 15 415–15 433, 2014.
- [4] P. J. G. Teunissen, "A new method for fast carrier phase ambiguity estimation," in *Position Location and Navigation Symposium*, 1994.
- [5] P. J. Teunissen, "The least-squares ambiguity decorrelation adjustment: a method for fast GPS integer ambiguity estimation," *J. Geodesy*, vol. 70, no. 1, pp. 65–82, 1995.
- [6] P. D. Jonge and C. Tiberius, "The LAMBDA method for integer ambiguity estimation: implementation aspects," *Delft Geodetic Computing Centre LGR Series*, vol. 12, 1996.
- [7] S. S. Hwang and J. L. Speyer, "Relative GPS carrier-phase positioning using particle filters with position samples," in *Amer. Control Conf.*, St. Louis, MO, Jun. 2009.
- [8] —, "Particle filters with adaptive resampling technique applied to relative positioning using GPS carrier-phase measurements," *IEEE Trans. Control Syst. Technol.*, vol. 19, no. 6, pp. 1384–1396, 2011.
- [9] M. Sahmoudi and R. Landry, "A nonlinear filtering approach for robust multi-GNSS RTK positioning in presence of multipath and ionospheric delays," *IEEE J. Sel. Topics Signal Process.*, vol. 3, no. 5, pp. 764–776, 2009.
- [10] K. Berntorp, A. Weiss, and S. Di Cairano, "GNSS ambiguity resolution by adaptive mixture Kalman filter," in *21st International Conference on Information Fusion*, Cambridge, UK, Jul. 2018.
- [11] K. Berntorp, A. Weiss, and S. Di Cairano, "Integer ambiguity resolution by mixture Kalman filter for improved GNSS precision," *IEEE Trans. Aerospace and Electronic Systems*, Feb. 2020.
- [12] F. Gustafsson, *Statistical Sensor Fusion*. Lund, Sweden: Utbildningshuset/Studentlitteratur, 2010.
- [13] S. M. Kay, *Fundamentals of statistical signal processing*. Prentice Hall PTR, 1993.
- [14] B. Azimi-Sadjadi and P. Krishnaprasad, "Integer ambiguity resolution in GPS using particle filtering," in *Amer. Control Conf.*, Arlington, VA, Jun. 2001.
- [15] G. Xu and Y. Xu, *GPS: theory, algorithms and applications*. Springer, 2016.
- [16] G. Blewitt, "Basics of the GPS technique: observation equations," *Geodetic Applications of GPS*, pp. 10–54, 1997.
- [17] J. Klobuchar, "Ionospheric time-delay algorithm for single-frequency GPS users," *IEEE Trans. Aerosp. Electron. Syst.*, vol. 3, no. 23, pp. 325–331, 1987.
- [18] J. Saastamoinen, "Contributions to the theory of atmospheric refraction," *Bull. G eod esique*, vol. 105, no. 1, pp. 279–298, 1973.
- [19] T. B. Sch on, F. Gustafsson, and P.-J. Nordlund, "Marginalized particle filters for mixed linear nonlinear state-space models," *IEEE Trans. Signal Process.*, vol. 53, pp. 2279–2289, 2005.
- [20] M. Arulampalam, S. Maskell, N. Gordon, and T. Clapp, "A tutorial on particle filters for online nonlinear/non-Gaussian Bayesian tracking," *IEEE Trans. Signal Process.*, vol. 50, no. 2, pp. 174–188, 2002.
- [21] F. Gustafsson, "Particle filter theory and practice with positioning applications," *IEEE Aerosp. Electron. Syst. Mag.*, vol. 25, no. 7, pp. 53–82, 2010.
- [22] C. M. Bishop, *Pattern Recognition and Machine Learning*. NJ, USA: Springer-Verlag New York, 2006.
- [23] K. B. Petersen, M. S. Pedersen *et al.*, "The matrix cookbook," *Technical University of Denmark*, vol. 7, no. 15, p. 510, 2008.